JACS
JOURNAL OF THE AMERICAN CHEMICAL SOCIETY

Communication

pubs.acs.org/JACS

Core Values: Elucidating the Role of Seed Structure in the Synthesis of Symmetrically Branched Nanocrystals

Christopher J. DeSantis and Sara E. Skrabalak*

Department of Chemistry, Indiana University, Bloomington, Indiana 47405, United States

Supporting Information

ABSTRACT: Branched metal nanoparticles often display unique physicochemical properties on account of their structures; however, most examples are asymmetric, with branches randomly distributed from the cores of the nanoparticles. This asymmetry can give rise to variable properties between samples. Here, we report the synthesis of symmetrically branched Au/Pd nanocrystals including five-branched pentapods with D_{3h} symmetry, 24-branched nanocrystals with O_h symmetry, 12-branched nanocrystals with T_d symmetry, and eight-branched octopods and bowties with O_h and D_{4h} symmetry, respectively. These structures are achieved by seed-mediated co-reduction wherein the shapes of the seeds direct the number and symmetry patterns of the branches. Compositional boundaries exist at the interfaces between the seed and overgrowth metals to provide visualization via advanced electron microscopy of the relationships between seed structure and the symmetry of branched nanocrystals. Significantly, seed structure plays a definitive role in determining the final shape of convex metal nanocrystals, and the results presented here illustrate a similar relationship for branched nanocrystals and will enable the design of new architecturally distinct nanostructures.

Branched metal nanoparticles such as nanostars and nanodendrites are exciting plasmonic and catalytic platforms on account of their often large surface areas, multiple high-angle edges, and sharp tips.[1] The small radius of curvature of sharp tips can concentrate electromagnetic fields at these features of Au and Ag nanostructures to achieve high sensitivity in plasmon-enhanced surface spectroscopies.[2−4] Also, through size-controlled syntheses of branched metal nanoparticles, the extinction features of their localized surface plasmon resonance (LSPR) can be tuned.[5,6] However, most branched metal nanoparticles are asymmetric. As a result, their properties are not as well-defined or precisely and reproducibly manipulated compared to nanostructures with defined symmetries.[7−12] Here, the role of seed structure in branched nanocrystal synthesis is elucidated by growing compositionally different branches from shape-controlled seeds. Elemental mapping of the resultant bimetallic structures allows the number and symmetry of the branches to be directly associated with the structural features of the seeds for the first time.[13,14] Whereas a paradigm toward convex nanocrystal synthesis has emerged with seeds of a particular structure leading to a limited number of shape-controlled nanocrystals,[15] the analogous model for concave and branched nanocrystals is incomplete.[16,17] Significantly, this seed-directed approach begins to fill in the gaps by enabling the synthesis of new symmetrically branched nanocrystals and providing a foundation for the rational design of concave nanostructures in general.

The uncertain relationship between seed structure and branched nanocrystal symmetry arises from difficulty in imaging the tiny seeds present during a synthesis and their subsequent ability to restructure during overgrowth. For example, CdTe tetrapods can be rationalized to form from either sphalerite octahedra or wurtzite pyramids based on crystal symmetry arguments, but the small sizes of the nanocrystal cores can preclude a definitive assignment.[18] Likewise, Pd/Pt nanodendrites have been synthesized from cuboctahedral Pd seeds, but the hyper-branched nature of the dendrites makes correlating their three-dimensional (3D) structures to the shape of the seeds difficult.[19] Finally, we reported the synthesis of eight-branched Au/Pd octopods with O_h symmetry by seed-mediated co-reduction, wherein Au and Pd precursors were co-reduced to deposit metal onto {111}-terminated octahedral Au seeds.[20] Both Au and Pd precursors are necessary as the co-reduction technique itself manipulates the kinetics of seeded growth in favor of branched nanocrystal formation rather than platonic core@shell nanocrystals.[20] However, the role of the seeds in directing overgrowth remains unclear.[21] Mainly, the branches of the Au/Pd octopods extend along the ⟨111⟩ directions from the cores of the nanostructures and suggest that growth occurs preferentially from the eight {111} facets of the octahedral seeds. Yet, crystal growth theory argues that growth rates should be greatest at the highest energy features of seeds; i.e., the six vertices of each octahedron. Thus, it was postulated in the original report that the Au seeds restructure during growth to cubic-like structures. Unfortunately, verifying this hypothesis is difficult in this system as Au deposits before Pd and provides no differentiation between the Au seeds and overgrowth metal. Lack of elemental distinction is common in nanocrystal syntheses and is overcome here by replacing the Au seeds with shape-controlled Pd nanostructures. This change provides compositional boundaries between the seed and overgrowth metals as Au deposits first onto the now Pd seeds and enables visualization of the relationship between seed structure and the symmetry of branched nanocrystals by electron microscopy (EM). In effect, the shape-controlled Pd nanocrystals serve as TEM labels, just as single-crystalline Au seeds were used to follow the growth of twinned Ag icosahedral shells.[22]

Received: August 25, 2012
Published: December 27, 2012

   dx.doi.org/10.1021/ja308456w | J. Am. Chem. Soc. 2013, 135, 10−13

Specifically, $HAuCl_4$ and H_2PdCl_4 were co-reduced with L-ascorbic acid (L-AA) in the presence of shape-controlled Pd seeds with either CTAB or CTAC/Br^- as a stabilizing agent. The Pd seeds included {100}-faceted nanocubes, nanobars, and right bipyramids as well as {111}-faceted octahedra and tetrahedra. All seeds were prepared by standard methods.[8,23,24] The concentrations of L-AA and CTA^+ were held constant for each synthesis, but the concentrations of $HAuCl_4$, H_2PdCl_4, and Br^- had to be optimized for each seed shape on account of their different surface areas and number of vertices per seed, which yields different numbers of branches per vertex depending on the shape. See details in Supporting Information. The co-reduction of Au and Pd precursors with Pd nanocubes as seeds (Figure 1A)

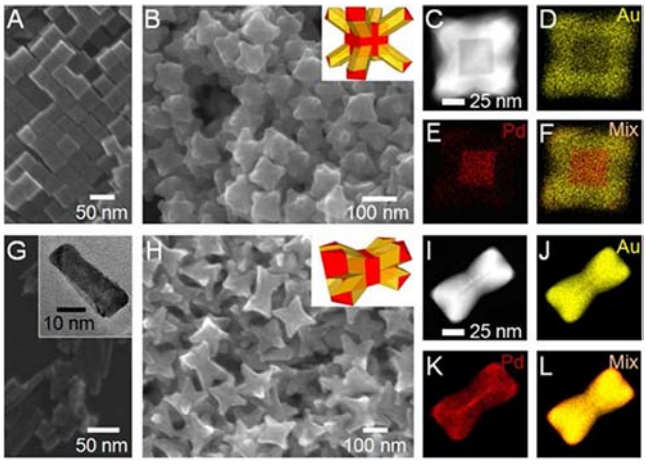

Figure 1. SEM images of (A) Pd nanocubes and (B) Au/Pd octopods (inset: a structural model). (C) A STEM image of a Au/Pd octopod and (D–F) elemental map by STEM-EDX analysis. Yellow, Au; red, Pd. SEM images of (G) Pd nanobars (inset: TEM image) and (H) Au/Pd bowties (inset: a structural model). (I) A STEM image of a Au/Pd bowtie and (J–L) elemental map by STEM-EDX analysis. Yellow, Au; red, Pd.

gives nanocrystals with eight branches and O_h symmetry (Figure 1B). Electron diffraction (ED) from two particles with different orientations confirms that the branches grow along the ⟨111⟩ directions (Figure S1A–D). Elemental mapping by STEM/EDX analysis (Figure 1C–F) shows that the nanocrystal cores consist of the Pd nanocubes, with no evidence of seed restructuring. Both elemental mapping and a TEM tilt study (Figure S2) show that the Au-based branches emerge from the eight vertices of each nanocube. Pd decorates the surfaces of the octopods as its deposition, which is required for branch formation, is temporally separated from that of Au.[21] A structural model is provided as an inset to Figure 1B. Likewise, Pd nanobars (Figure 1G) also yield eight-branched nanocrystals (Figure 1H), only now with bowtie-like particle architectures and D_{4h} symmetry that is consistent with the long axis of the nanobar seeds. Elemental mapping by STEM/EDX analysis shows that branching occurs again from the vertices of intact Pd seeds (Figure 1I–L), and ED indicates that the branches proceed along the ⟨111⟩ directions (Figure S1E,F). A structural model is in the inset to Figure 1H.

Right bipyramids are an impurity in some Pd nanocube syntheses and result from a (111) twin plane being introduced.[25,26] They express six {100}-facets and five vertices (Figure 2A). Interestingly, five-branched pentapods with trigonal bipyramidal D_{3h} symmetry are produced from co-reducing Au and Pd precursors in the presence of these seeds (Figure 2B). A

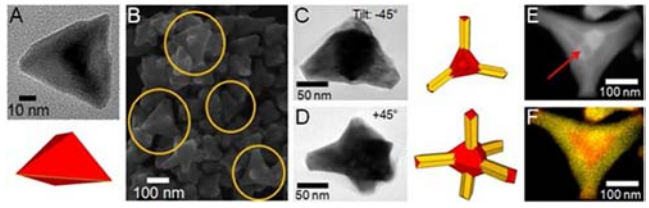

Figure 2. (A) A TEM image of a Pd right bipyramid and structural model below. (B) A SEM image of Au/Pd pentapods. (C, D) TEM images of a pentapod at two perspectives to reveal the in-plane (top) and axial (bottom) branches; structural models included. (E) A STEM image of a pentapod with the fifth branch projected toward the TEM grid and (F) elemental mapping by STEM/EDX analysis. Yellow, Au; red, Pd.

TEM tilt study of a particle reveals the three in-plane and two axial branches of a pentapod (Figure 2C,D). Structural models are included. Elemental mapping by STEM/EDX analysis indicates that overgrowth occurs again from the vertices of the Pd seeds (Figure 2E,F). The ED pattern obtained from a pentapod positioned with axial branches parallel with the electron beam is close to the [111] zone axis and consistent with the axial branches extending along ⟨111⟩ directions perpendicular to the (111) twin plane of the Pd seed (Figure S3). Considering the in-plane branches, they are each 90° from the axial branches and at 120° from one another. Thus, the in-plane branches proceed along ⟨112⟩ directions (Figure S3). Tilting an in-plane branch of a pentapod toward the [110] zone axis reveals that the twin plane that bisects the Pd right bipyramidal seeds extends the lengths of the branches (Figures 3

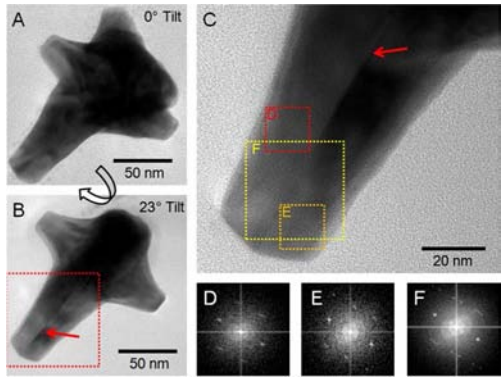

Figure 3. TEM images of a pentapod at (A) 0° and (B) 23° tilt (arrow denotes location of twin plane). (C) Higher magnification TEM image of region from (B). (D–F) FFTs of regions in (C).

and S4 for a second example). FFTs of the regions on each side of the twin are nearly mirror images (Figure 3D–F), and lattice spacings of 0.22 nm are measured at the same angle on each side of the twin (Figure S5).[27] A trend is evident from the results obtained with the use of {100}-terminated Pd seeds: one branch emerges from each seed vertex. Fundamentally, nucleation and growth is preferential at the highest energy features of the seeds.

To test if this trend is general to branched metal nanocrystal formation, {111}-terminated Pd nanocrystals were also used as seeds. From octahedra (Figure 4A), particles with complex and asymmetric branching were obtained from preliminary experiments (Figure S6). SEM of the structures revealed poorly developed branches which we ascribed to insufficient space for their growth. Thus, the Br^- concentration in the synthesis was

dx.doi.org/10.1021/ja308456w | J. Am. Chem. Soc. 2013, 135, 10–13

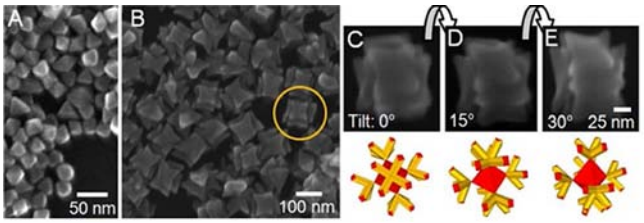

Figure 4. SEM images of (A) Pd octahedra and (B–E) 24-branched Au/Pd nanocrystals. In (B), a particle oriented with four branches away from the substrate is circled. (C–E) SEM images of a particle that is tilted by 15° then 30° to reveal another set of four branches (models below).

optimized by replacing CTAB with CTAC and adding back Br^- in lower amounts as this procedure was previously shown to produce metal nanocrystals with thinner branches and sharper tips.[21] 24-branched nanocrystals with O_h symmetry were achieved (Figure 4B). A particle oriented on the imaging substrate for structural analysis is circled and reveals four branches positioned away from the substrate much like with the octopods and bowties. Four regions of additional overgrowth are evident from the sides of the particle. Tilting a similar particle in 15° increments during SEM revealed that the side overgrowths also consist of four branches (Figure 4C–E). STEM imaging, elemental mapping, and ED indicate that the branches grow along ⟨111⟩ directions, with four branches beginning from each vertex of an octahedron for a total of 24 branches (Figures S7, S8).[28] Models are included in Figures 4 and S8.

Quenching this growth process as a function of reaction time then analyzing the samples by EM further confirms preferential nucleation at the seed vertices (Figure S9). After 1 min, metal collects at some of the vertices of the octahedra but branching is not observed (Figure S9A,B). Lattice registration and an epitaxial relationship between the seed and overgrowth metals are evident as is also the case when the metal precursor concentrations are decreased relative to that of the seeds (Figure S10). By 3 min, anisotropic growth from the initial site of metal deposition is evident (Figure S9C,D). The 24-branched nanocrystals form within 10 min (Figure S9G). Just as with the {100}-terminated Pd seeds, overgrowth occurs preferentially where surface energy is highest, i.e., the vertices. The emergence of four branches from each vertex rather than one also signifies that branched growth is not merely dependent upon the number of vertices and will enable new branched crystals to be envisioned.

To evaluate the possibility of other branching patterns, Pd tetrahedra were also used as seeds (Figure 5A). Again, structures with more branches then seed vertices form (Figure 5B).

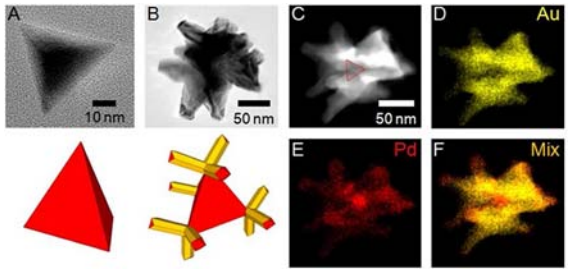

Figure 5. (A) A TEM image of a Pd tetrahedron and corresponding model below. (B) A TEM image of a multibranched Au/Pd nanocrystal and proposed model below. (C) A STEM image of a multibranched Au/Pd nanocrystal and (D–F) corresponding STEM/EDX elemental mapping. Yellow, Au; red, Pd.

Elemental mapping by STEM-EDX analysis confirms the presence of Pd cores and the emergence of multiple branches per vertex (Figure 5C–F). A TEM tilt study of an individual particle in 15° increments reveals that three branches emerge per vertex although only three of the overgrowth regions can be fully imaged due to the fourth being positioned on the imaging substrate (Figure S11). From the crystallographic orientation of a tetrahedral nanocrystal, we propose that the branches proceed again along ⟨111⟩ directions for a total of 12 branches per particle and T_d symmetry (see Scheme S1 and models in Figures 5, S11).

From the data presented, two parameters are identified as significant to branched metal nanocrystal growth: (1) the number of seed vertices and (2) the growth directions of the branches. The former reflects the preference for nucleation and growth to originate from the vertices of the nanocrystals and can be rationalized in terms of surface energy; i.e., the growth rate will be greatest at the highest energy features under kinetically controlled growth conditions.[29] This idea is represented in Scheme S2 as Stage 1.

The latter reflects the preference for 1-D growth to proceed along ⟨111⟩ directions of single-crystalline seeds (i.e., those without twins or other defects) regardless of shape and is shown in Scheme S2 as Stage 2. The origin of this trend is less obvious and may be attributed to several factors. For example, the 1-D growth of Au nanorods is rationalized both in terms of surface stabilization and minimization of strain, and these factors may be relevant to the synthesis of symmetrically branched nanocrystals. Specifically, CTAB is thought to minimize the surface energy of the {100}/{110} side facets of Au nanorods and facilitate their expression relative to the poorly stabilized {111} ends,[30] and the branches of the nanocrystals reported here have similarities to Au nanorods. Also, the decahedral seeds from which some Au nanorods originate can be thought of as five tetrahedral single-crystals joined with {111} twin planes. An atom deficient gap is accommodated by bond elongation, and lateral growth rather than axial would increase internal lattice strain.[15] With the exception of the right bipyramids, the seeds used in these syntheses do not have such structural defects, but there is a ~4% lattice mismatch between Pd and Au and this difference may facilitate anisotropic growth as a means of minimizing strain when Au deposits on the Pd cores. Such nonconformal growth was observed in Yang and coworkers' study of heteroepitaxial deposition in 3-D and could account for the differences we observed with the use of Au and Pd octahedra.[31]

Although these factors may account for branch formation generally, they do not account fully for our observations. For example, the vertices of both the cubic and tetrahedral seeds can accommodate more branches along ⟨111⟩ directions (e.g., in addition to the three branches that proceed normal to the side facets of a tetrahedron, a fourth branch could proceed in the ⟨111⟩ direction normal to the base facet). Our preliminary analysis suggests that the acuteness of the vertices coupled with the crystallographic orientation of the vertices relative to available growth directions accounts for the different number of branches emerging per vertex depending on seed shape. We also note that the number and acuteness of the vertices per seed may limit the number of branches that can form due to overcrowding. This idea is reflected in our preliminary study of octahedral seeds (Figure S6) and in our results obtained with cuboctahedral Pd seeds (Figure S12A) which gave nanocrystals with intricate branching patterns (Figure S12B). There is good uniformity in structure but the individual branch lengths and widths vary. Elemental mapping confirms the presence of the Pd

dx.doi.org/10.1021/ja308456w | J. Am. Chem. Soc. 2013, 135, 10–13

core although its orientation relative to the branching pattern could not be verified (Figure S12C−H). EM tilt studies of individual particles highlight the difficulty in assigning symmetry due to multiple branches emerging from the many vertices of each seed (Figure S13). Future efforts will focus on decoupling factors such as defect structure (i.e., twinning), lattice mismatch between seed and overgrowth metal as well as vertex angles so that branch growth can proceed predictably in many directions.

On account of their composition, symmetry, and sharp tips, these nanocrystals are intriguing platforms for the study of Pd/adsorbate interactions by plasmon-enhanced surface spectroscopy.[32] See Supporting Information and Figures S14 and S15 for full discussion. Moreover, seed structure is known to play a critical role in the synthesis of convex shape-controlled nanocrystals and core@shell nanocrystals,[33−35] and understanding its role in concave and branched nanocrystal synthesis will enable new nanocrystals with well-defined structures and properties to be achieved. Here, a general route to symmetrically branched metal nanocrystals is outlined, wherein the shape of the initial seeds determines the overgrowth process by providing referential sites for branched growth. This research focused on a model Au/Pd system to provide direct visualization of the seed-symmetry relationships but we anticipate that the principles outlined will hold for other systems as well.

■ ASSOCIATED CONTENT

Supporting Information

Experimental procedures, additional characterization, and a movie from a TEM tilt study. This material is available free of charge via the Internet at http://pubs.acs.org.

■ AUTHOR INFORMATION

Corresponding Author

sskrabal@indiana.edu

Notes

The authors declare no competing financial interest.

■ ACKNOWLEDGMENTS

Support from Indiana University and the Cottrell Scholar Program (Research Corporation). Tetrahedral Pd seeds provided by Yan Dai of Dr. Nenfang Zhang's group at Xiamen University, China. Thanks to Dr. David Morgan for assistance with TEM, IU Nanoscale Characterization Facility instrument access, and Professors Liang-shi Li and Emilie Ringe for their discussions.

■ REFERENCES

(1) Lim, B.; Xia, Y. *Angew. Chem., Int. Ed.* **2011**, *50*, 76.
(2) Hao, F.; Nehl, C. L.; Hafner, J. H.; Nordlander, P. *Nano Lett.* **2007**, *7*, 729.
(3) Khoury, C. G.; Vo-Dinh, T. *J. Phys. Chem. C* **2008**, *112*, 18849.
(4) Kumar, P. S.; Pastoriza-Santos, I.; Rodríguez-González, B.; Abajo, F. J. G. d.; Liz-Marzán, L. M. *Nanotechnology* **2008**, *19*, 015606.
(5) DeSantis, C. J.; Skrabalak, S. E. *Langmuir* **2012**, *28*, 9055.
(6) Barbosa, S.; Agrawal, A.; Rodríguez-Lorenzo, L.; Pastoriza-Santos, I.; Alvarez-Puebla, R. n. A.; Kornowski, A.; Weller, H.; Liz-Marzán, L. M. *Langmuir* **2010**, *26*, 14943.
(7) Kim, D. Y.; Yu, T.; Cho, E. C.; Ma, Y.; Park, O. O.; Xia, Y. *Angew. Chem., Int. Ed.* **2011**, *50*, 6328.
(8) Huang, X.; Tang, S.; Zhang, H.; Zhou, Z.; Zheng, N. *J. Am. Chem. Soc.* **2009**, *131*, 13916.
(9) Mulvihill, M. J.; Ling, X. Y.; Henzie, J.; Yang, P. *J. Am. Chem. Soc.* **2009**, *132*, 268.
(10) Dai, Y.; Mu, X.; Tan, Y.; Lin, K.; Yang, Z.; Zheng, N.; Fu, G. *J. Am. Chem. Soc.* **2012**, *134*, 7073.
(11) Hong, J. W.; Lee, Y. W.; Kim, M.; Kang, S. W.; Han, S. W. *Chem. Commun.* **2011**, *47*, 2553.
(12) Xia, X.; Zeng, J.; McDearmon, B.; Zheng, Y.; Li, Q.; Xia, Y. *Angew. Chem., Int. Ed.* **2011**, *50*, 12542.
(13) Wang, F.; Li, C.; Sun, L.-D.; Wu, H.; Ming, T.; Wang, J.; Yu, J. C.; Yan, C.-H. *J. Am. Chem. Soc.* **2010**, *133*, 1106.
(14) Lu, C.-L.; Prasad, K. S.; Wu, H.-L.; Ho, J.-a. A.; Huang, M. H. *J. Am. Chem. Soc.* **2010**, *132*, 14546.
(15) Xia, Y.; Xiong, Y.; Lim, B.; Skrabalak, S. E. *Angew. Chem., Int. Ed.* **2009**, *48*, 60.
(16) Zhang, H.; Jin, M.; Xia, Y. *Angew. Chem., Int. Ed.* **2012**, *51*, 7656.
(17) Maksimuk, S.; Teng, X.; Yang, H. *J. Phys. Chem. C* **2007**, *111*, 14312.
(18) Carbone, L.; Kudera, S.; Carlino, E.; Parak, W. J.; Giannini, C.; Cingolani, R.; Manna, L. *J. Am. Chem. Soc.* **2005**, *128*, 748.
(19) Lim, B.; Jiang, M.; Camargo, P. H. C.; Cho, E. C.; Tao, J.; Lu, X.; Zhu, Y.; Xia, Y. *Science* **2009**, *324*, 1302.
(20) DeSantis, C. J.; Peverly, A. A.; Peters, D. G.; Skrabalak, S. E. *Nano Lett.* **2011**, *11*, 2164.
(21) DeSantis, C. J.; Sue, A. C.; Bower, M. M.; Skrabalak, S. E. *ACS Nano* **2012**, *6*, 2617.
(22) Langille, M. R.; Zhang, J.; Personick, M. L.; Li, S.; Mirkin, C. A. *Science* **2012**, *337*, 954.
(23) Zhang, J.; Zhang, L.; Xie, S.; Kuang, Q.; Han, X.; Xie, Z.; Zheng, L. *Chem.— Eur. J.* **2011**, *17*, 9915.
(24) Hong, J. W.; Kim, D.; Lee, Y. W.; Kim, M.; Kang, S. W.; Han, S. W. *Angew. Chem., Int. Ed.* **2011**, *50*, 8876.
(25) Wiley, B. J.; Xiong, Y.; Li, Z.-Y.; Yin, Y.; Xia, Y. *Nano Lett.* **2006**, *6*, 765.
(26) Zhang, J.; Li, S.; Wu, J.; Schatz, G. C.; Mirkin, C. A. *Angew. Chem., Int. Ed.* **2009**, *48*, 7787.
(27) Lim, B.; Jiang, M.; Tao, J.; Camargo, P. H. C.; Zhu, Y.; Xia, Y. *Adv. Funct. Mater.* **2009**, *19*, 189.
(28) Kim, M.-J.; Cho, Y.-S.; Park, S.-H.; Huh, Y.-D. *Cryst. Growth Des.* **2012**, *12*, 4180.
(29) Langille, M. R.; Personick, M. L.; Zhang, J.; Mirkin, C. A. *J. Am. Chem. Soc.* **2011**, *133*, 10414.
(30) Gao, J.; Bender, C. M.; Murphy, C. J. *Langmuir* **2003**, *19*, 9065.
(31) Habas, S. E.; Lee, H.; Radmilovic, V.; Somorjai, G. A.; Yang, P. *Nat. Mater.* **2007**, *6*, 692.
(32) Fang, P.-P.; Jutand, A.; Tian, Z.-Q.; Amatore, C. *Angew. Chem., Int. Ed.* **2011**, *50*, 12184.
(33) Jin, M.; Zhang, H.; Wang, J.; Zhong, X.; Lu, N.; Li, Z.; Xie, Z.; Kim, M. J.; Xia, Y. *ACS Nano* **2012**, *6*, 2566.
(34) Yang, C.-W.; Chanda, K.; Lin, P.-H.; Wang, Y.-N.; Liao, C.-W.; Huang, M. H. *J. Am. Chem. Soc.* **2011**, *133*, 19993.
(35) Xia, Y.; Xiong, Y.; Lim, B.; Skrabalak, S. E. *Angew. Chem., Int. Ed.* **2009**, *48*, 60.